Case Studies in Thermal Engineering 52 (2023) 103810

Contents lists available at ScienceDirect

Case Studies in Thermal Engineering

journal homepage: www.elsevier.com/locate/csite

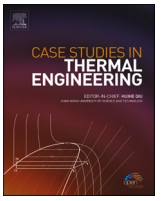

Numerical analysis of multipurpose shell-tube-heat exchanger withal stylized geometry at different baffle gaps and various flow rates

Mehmet Akif kartal [a,*], Ahmet feyzioğlu [b]

[a] Bandırma Onyedi Eylül University, Distance Education Application and Research Center, 10200, Bandırma, Balıkesir, Turkey
[b] Marmara University, Technology Faculty, Mechanical Engineering, Production Planning and Control Department, 34722, Kadıköy, İstanbul, Turkey

ARTICLE INFO

Keywords:
Exchanger
Baffle board
CFD
Computational

ABSTRACT

The effects of changing 90 mm and 110 mm plate spacings and FR factor of 0.9 kg/h, 1.3 kg/h, 1.7 kg/h, 1.9 kg/h on the total heat transfer performance and PD in the new design HX were examined. The results obtained by taking into account the change in plate spacing and FR factor of 0.9 kg/h, 1.3 kg/h, 1.7 kg/h and 1.9 kg/h, as well as variable factors, were transferred to the study and displayed in figures. In the study, firstly, the results of HCO obtained by changing FR and range were monitored. In the analysis, the interval values were 90 mm and 110 mm and the changes in the FR values of 0.9 kg/h, 1.3 kg/h, 1.7 kg/h and 1.9 kg/h increased in direct proportion. The smallest value of the heat transfer rate was obtained at 110 mm plate spacing and 0.9 kg/h FR. In addition, if the plate spacing was 90 mm, the smallest HCO was obtained at 0.9 kg/h. The largest HCO was obtained when the plate spacing was 90 mm and FR was 1.9 kg/h. In the second part of the study, the results of PD obtained by changing FR and gap were monitored. In the analysis, the interval values were 90 mm and 110 mm and the changes in FR values of 0.9 kg/h, 1.3 kg/h, 1.7 kg/h and 1.9 kg/h increased in direct proportion. The smallest value of PD level was obtained at 90 mm plate spacing and 0.9 kg/h FR. In addition, if the plate spacing was 110 mm, the smallest heat transfer coefficient was obtained at 0.9 kg/h. The largest PD value was obtained when the plate spacing was 110 mm and FR was 1.9 kg/h. In the last part of the study, the results obtained by changing FR and range of the HTPD value were monitored. In the analysis, the interval values were 90 mm and 110 mm, and the changes in FR values of 0.9 kg/h, 1.3 kg/h, 1.7 kg/h and 1.9 kg/h decreased in direct proportion. The smallest value of the HTPD level was obtained at 110 mm plate spacing and 1.9 kg/h FR. In addition, if the plate spacing was 90 mm, the smallest HTPD value was obtained at 1.9 kg/h. The highest HTPD value was obtained when the plate spacing was 90 mm and FR was 0.9 kg/h. Therefore, choosing a system with a 90 mm plate spacing and a FR of 0.9 kg/h will be more efficient in terms of thermohydraulic performance and pressure balancing. As a result, it was concluded that if the plate spacing was selected as 90 mm, a 15 % improvement could be achieved compared to the system design with a 110 mm plate spacing. As a new, it is thought that it will contribute to the literature in future studies, as the thermal performance, pressure drop and heat transfer coefficient results obtained at new flow rate values and compartment spacing values are obtained for the first time in a new STH designed in different dimensions than the literature.

* Corresponding author.
E-mail address: mkartal@bandirma.edu.tr (M. Akif kartal).

https://doi.org/10.1016/j.csite.2023.103810
Received 4 August 2023; Received in revised form 7 November 2023; Accepted 20 November 2023
Available online 23 November 2023

1. Introduction

Although HXs have created a wide usage network in many sectors, starting from chemical and industry-based manufacturing and process industries [1], various studies have been carried out to increase thermal performance and, on the contrary, reduce flow resistance [2]. In addition to the use of shaped pipes [3] rather than straight pipes to increase heat transfer in HX type and CFD studies being an effective tool in predicting the behavior of various HXs [4], various studies are also carried out on BFFs. The most striking of these was the development of BFFs in different types and patterns [5]. Efficiency in heat transfer has increased thanks to BFFs that play a role in changing fluid behavior and improving heat transfer [6]. The use of the K-Epsilon turbulence model has provided better results in shell and tube exchangers [7]. They observed that the performance of BFF of the model developed by Tong et al. was 19.5 % better than that of the conventionally manufactured one [8].

Thanks to the direction plates, the liquid flow can be ensured in a zigzag and curved pattern. They also help improve heat transfer capacity by increasing the turbulence intensity and local mixing on the shell side. However, some inherent disadvantages can also be mentioned due to the structural limitations of sectional baffles, such as the tendency for severe fouling and the short operating life resulting from the high risk of vibration failure on the pipe bundle [9]. BFF types have different effects on heat transfer. For example, in terms of the benefits to be achieved in a HX manufactured in a helical structure, there are positive benefits such as reducing the contamination on the shell side, application to high viscosity fluid, increasing heat transfer performance and preventing vibration caused by flow [10]. Experimental and numerical research has been carried out on BFFs and the heat performance results they affected have been reported in the literature [11]. Various optimization methods have also been used to obtain the thermal performance and pressure effects of BFFs [12]. Additionally, studies have been conducted in which the effect of heat transfer media was also taken into account and observed together with BFFs [13].

In the study of Geete et al. the concepts of entropy, exergy and entrans were applied to investigate the yield of the constructed HX at dissimilar FRs and inlet temperatures of hot and cold fluids. After the analysis, operating conditions are recommended that provide the least amount of entropy, exergy and input loss, but where the efficiency should be as high as possible. As a result, the proposed conditions are; hot or cold fluent FRs should be 0.001/0.037 kg/s and inlet temperatures should be 59/26.8 °C, orderly [14]. In another research, a shell-tube type HX was designed according to the Kern method. Maximum efficiency value, minimum entropy production, input distribution and input-based thermal resistance values were found and real operating conditions were determined [15]. In the research study carried out for the optimization of HX, the optimum size of the counter-flow surface condenser was found by using entropy, exergy and entransy theories. It is observed that when the 4L/D ratio increases by one unit, the EDN amounts reduce by 0.05–0.02, but after a while, when the ratio increases by ten units, the EDN amounts decrease by only 0.01, and for the surface capacitor, the optimum condition of the ratio is 40 [16]. In the experimental study conducted by Nie et al. on STH, they determined that the helix angle of 40° was the value that gave the best results in terms of other angles analyzed [17]. In the study conducted by Taher et al. as a result of optimizing the pressure drop and fouling factors in the traditionally designed HX, it was possible to increase the performance by using helical baffles in the traditional baffle plate HX [18]. According to the numerical and experimental studies carried out by Chu et al. analyzes were carried out with three different types of HX models designed for partition plates: single-double layer and conventional. As a result, they observed that the two-layer helical baffle plate had a better performance than other single-layer and conventionally designed model HXs [19]. Das and his colleagues carried out their studies on the thermal performance of circular and elliptical pipes. Accordingly, they determined that the thermal performance of elliptical pipes was at a better level than that of other circular types of pipes [20].

2. Material and method

Three-dimensional analyzes were implemented through the agency of the computational fluid dynamics technique and by entry the required boarding conditions into the analysis.

2.1. Somatic model

It is possible to change properties such as heat transfer capacity, fluid behavior and PD according to the characteristics of the aforethought HX. In addition, heat transfer performance and PD can be planned and optimized with the placement design number of baffle boards and other typical features. It is used in the study was designed as a single pipe pass withal a lengthiness of 1300 mm and a diameter of 120 mm and is shown in Fig. 1.

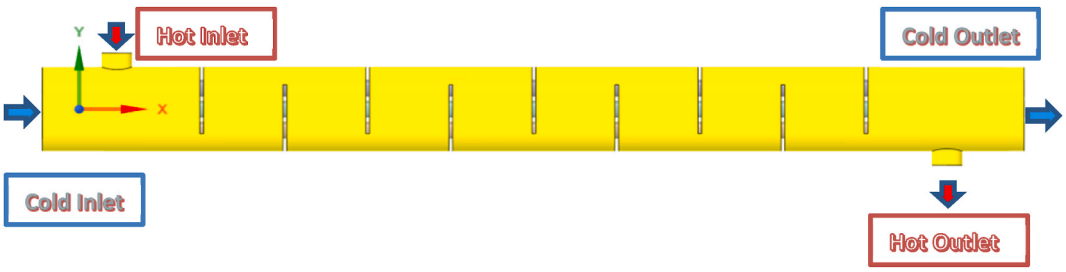

Fig. 1. Running water route.

The fact that the modification in the shape, arrangement and count of BFFs plays an considerable act in the fluid behavior, total heat transfer coefficient and PD becomes important during the design phase. While the details on which the measurements were made are shown in Table 1, the designed system including the entire body is shown in Fig. 2, and the details of the simulated dimensional measurements of BFFs are shown in Fig. 3.

2.2. Equations in study

The state of the fluid and the construction structure of the model in which it plays an important role in selecting the turbulence model. At this point, there is more than one turbulence model in the finite element method. In the study, the results were transferred to the study using the Realizable k-ε turbulence model. The equations used are given below [21]:

Momentum and energy equation:

$$A = -\frac{1}{\rho}\frac{\partial \mathrm{p}}{\partial \mathrm{x_i}} + \frac{\partial}{\partial \mathrm{x}_j}\left((\upsilon + \upsilon_\mathrm{t})\left(\frac{\partial \mathrm{u}_j}{\partial \mathrm{x_i}} + \frac{\partial \mathrm{u}_i}{\partial \mathrm{x_j}}\right)\right) \quad \frac{\partial \mathrm{u_i}\, T}{\partial \mathrm{x_i}} = \rho \frac{\partial}{\partial \mathrm{x}_i}\left(\left(\frac{\upsilon}{Pr} + \frac{\upsilon \mathrm{t}}{Pr}\right)\frac{\partial T}{\partial \mathrm{x_i}}\right) \tag{1}$$

Turbulent kinetic energy (k) and turbulent energy dissipation (ε) part:

$$\frac{\partial \mathrm{u_i}\, k}{\partial \mathrm{x_i}} = \frac{\partial}{\partial \mathrm{x}_i}\left[\left(\upsilon + \frac{\upsilon \mathrm{t}}{\sigma_k}\right)\frac{\partial k}{\partial \mathrm{x_i}}\right] + \Gamma - \varepsilon \quad \frac{\partial \mathrm{u_i}\varepsilon}{\partial \mathrm{x_i}} = \frac{\partial}{\partial \mathrm{x}_i}\left[\left(\upsilon + \frac{\upsilon \mathrm{t}}{\sigma_\varepsilon}\right)\frac{\partial \varepsilon}{\partial \mathrm{x_i}}\right] + \mathrm{c_1}\Gamma\varepsilon - \mathrm{c_2}\frac{\varepsilon^2}{k + \sqrt{\upsilon\varepsilon}} \tag{2}$$

Production of turbulent kinetic energy k; with "Γ" is shown in Equation (2) and Equation (3). C_μ is a function of mean strain and rotational speed.

$$\Gamma = -\overline{\mathrm{u_i}\,\mathrm{u_j}}\frac{\partial \mathrm{u_i}}{\partial \mathrm{x_i}} = \upsilon_\mathrm{t}\left(\left(\frac{\partial \mathrm{u}_i}{\partial \mathrm{x}_j} + \frac{\partial \mathrm{u}_j}{\partial \mathrm{x}_i}\right)\frac{\partial \mathrm{u}_i}{\partial \mathrm{x_i}}\right)\upsilon_\mathrm{t} = \mathrm{c}_\mu \frac{k^2}{\varepsilon} \tag{3}$$

Heat transfer rate (h_s):

$$h_s = \frac{[BodyHeatTransfer = Q_s = \dot{m}_s \bullet cp, s \bullet (Ts, i - Ts, o)]}{As = N \bullet \pi \bullet d_0 \bullet L \bullet \left(\frac{\left[T_{s,i} - T_w\right] - \left[T_{s,o} - T_w\right]}{ln\frac{\left[T_{s,i} - T_w\right]}{\left[T_{s,o} - T_w\right]}}\right)} \tag{4}$$

2.3. Boundary circumstances

In the study, the computational fluid dynamics method was used using standard wall functions. Therefore, standard wall functions are required to get more accurate results. The temperature of hot fluid intake the system was analyzed as 305 K and the temperature of the fluid intake the pipes was analyzed as 279 K. The necessary determinations were made on fluid behavior and PD, as BFF spacing was chosen as 90 mm and 110 mm, while ignoring environmental temperature loss and leaks. Fluid behavior at four different FRs such as 0.9 kg/h, 1.3 kg/h, 1.7 kg/h and 1.9 kg/h at two different plate spacing values was simulated and the results were transferred to the study.

2.4. Mesh independence test

In order to ensure the correctness of the analyses, the independence test, in which changes are presented depending on the number of mesh elements, becomes important. Accordingly, in models consisting of five different network systems with 294,284, 293,961, 295,161, 292,495 and 293,936 mesh elements grids were created and analyzed. Since the outlet temperature difference between the last two network systems was less than 1 %, it was concluded that the mesh grid structure with 292,495 elements was sufficient for the flow analyzes were carried out according to it. Fig. 4 simulates the analysis results.

3. Results and discussions

In the designed model, BFF of HXs with two different spacings of 90 mm and 110 mm were analyzed at four different FRs and transferred to the study together with their comparisons. Different fluid behaviors were obtained in modeling at FRs of 0.9 kg/h, 1.3 kg/h, 1.7 kg/h and 1.9 kg/h. As the fluid behavior changes, the topographic structure and turbulence map of PDs also change. Therefore, the total heat transfer coefficient and energetic performance differ. These changes are shown between Figs. 9 and 20. In summary, if FR is 0.9 kg/h, 1.3 kg/h, 1.7 kg/h and 1.9 kg/h and the baffle spacing is 90 mm, the temperature and pressure distributions

Table 1
Full measurements.

Definition	Size	Definition	Size	Definition	Size
Body		**Pipe**		**Baffle**	
R (mm)	60	D (mm)	24	Number	9
Length (mm)	1300	Sum	5	Thickness (mm)	5
Passes	1	Distance (mm)	6	Openness (mm)	90, 110

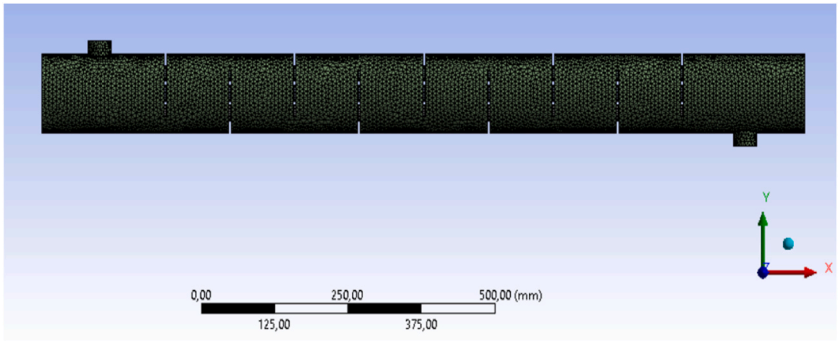

Fig. 2. Full body mesh section system.

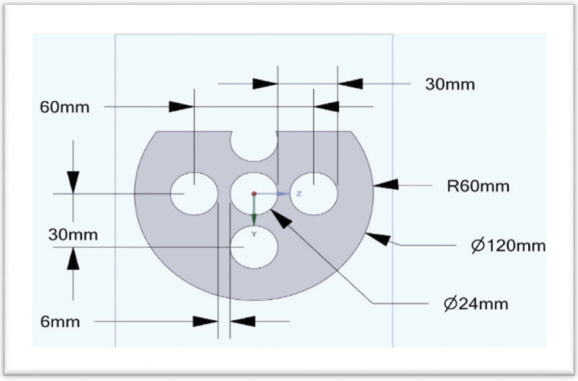

Fig. 3. Dimensional baffles.

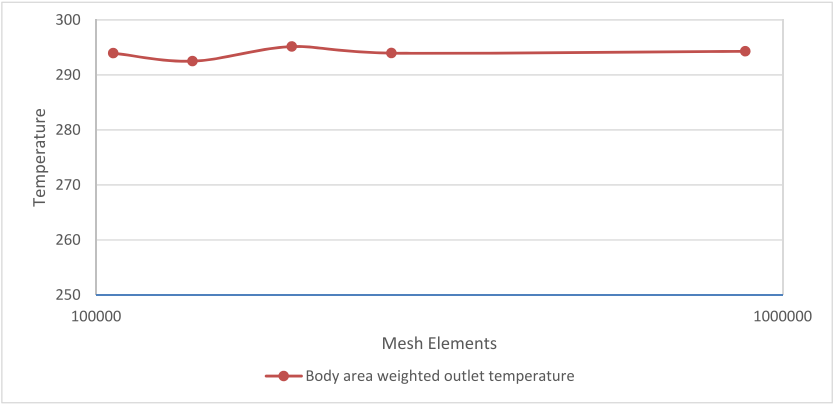

Fig. 4. Mesh independence test.

are different from those obtained when the BFF spacing is 110 mm. These differences are shown in Figs. 5–8.

Analyzes on the outlet temperature show that the outlet temperatures in the system with a plate spacing of 90 mm are lower than when the spacing is 110 mm. Additionally, if the plate spacing is 90 mm and FR are 0.9 kg/h, 1.3 kg/h, 1.7 kg/h and 1.9 kg/h, PD occurs at higher levels as the plate spacing increases and reaches 110 mm. According to another result, it was determined that the output level was lower in the case of 90 mm spacing and FRs of 0.9 kg/h, 1.3 kg/h, 1.7 kg/h and 1.9 kg/h.

According to Fig. 5, while the water temperature at the inlet side is between 278,963 °C and 285,276 °C, when the flow rate is 0.9 kg/h and the baffle gap is 90 mm, the cold water interacts with the hot water and the cold water towards the outlet heats up approximately due to heat exchange. It is observed that it reaches 304,216 °C.

In the other case, according to Fig. 8, while the water temperature on the inlet side is between 279,000 °C and 286,879 °C, when the flow rate is 0.9 kg/h and the baffle gap is 110 mm, the cold water interacts with the hot water and cold water towards the outlet due to

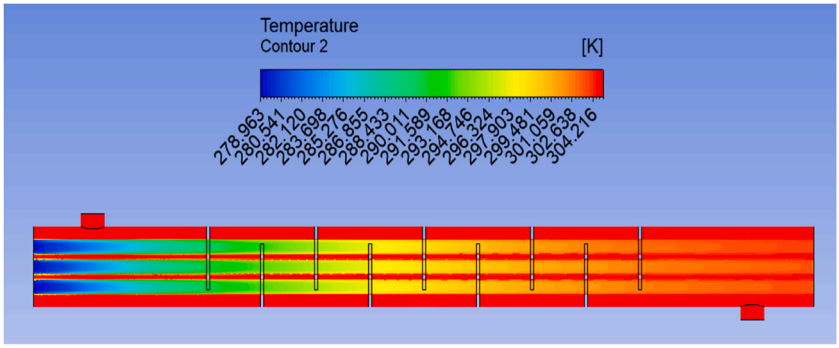

Fig. 5. Temperature distribution of the system interval = 90 mm, Flowrate = 0.9 kg/h.

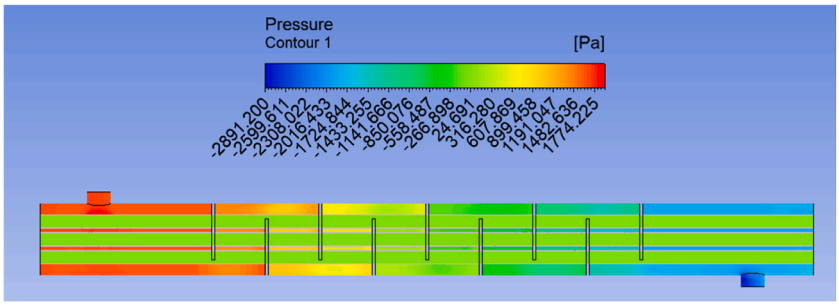

Fig. 6. Pressure distribution of the system interval = 90 mm, Flowrate = 0.9 kg/h.

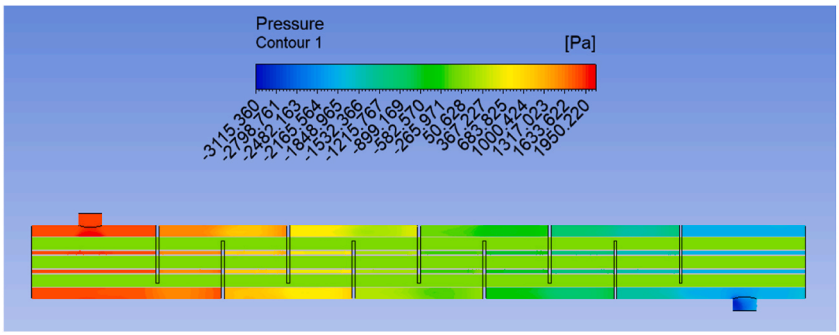

Fig. 7. Pressure distribution of the system interval = 110 mm, Flowrate = 0.9 kg/h.

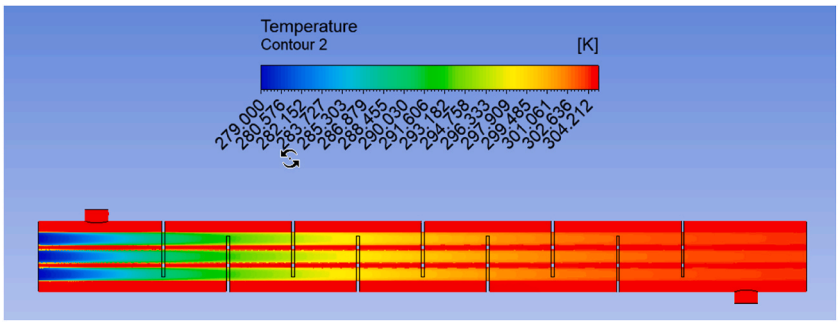

Fig. 8. Temperature distribution of the system interval = 110 mm, Flowrate = 0.9 kg/h.

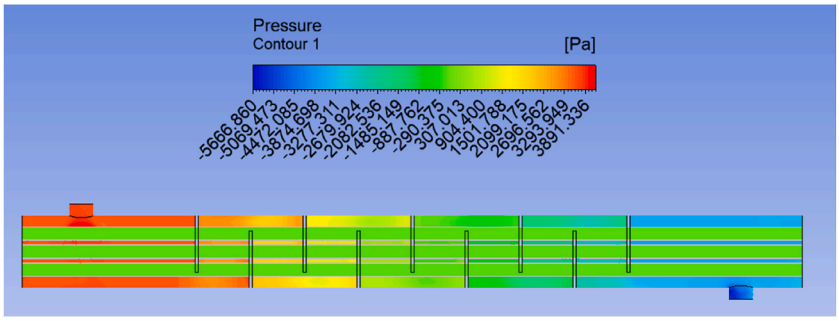

Fig. 9. Pressure distribution of the system interval = 90 mm, Flowrate = 1.3 kg/h.

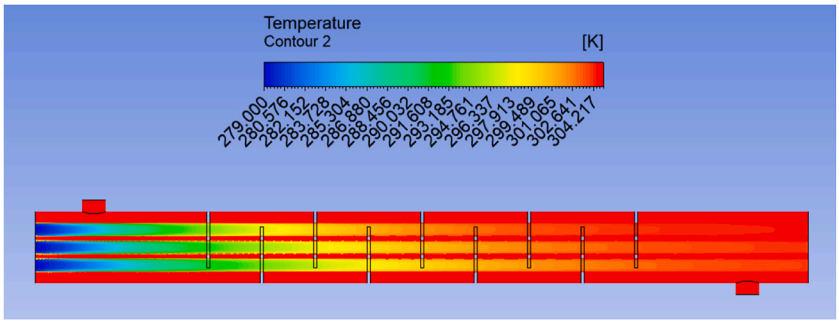

Fig. 10. Temperature distribution of the system interval = 90 mm, Flowrate = 1.3 kg/h.

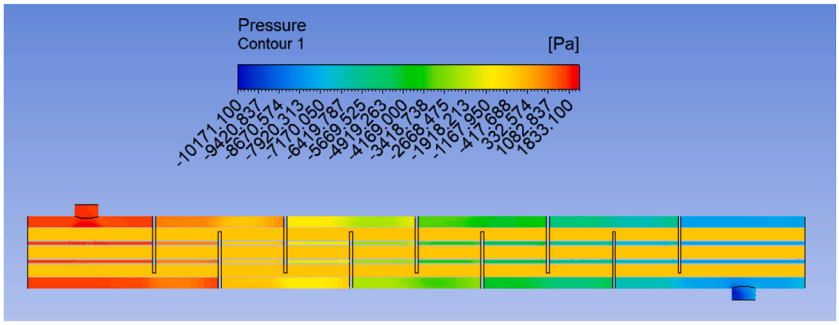

Fig. 11. Pressure distribution of the system interval = 110 mm, Flowrate = 1.3 kg/h.

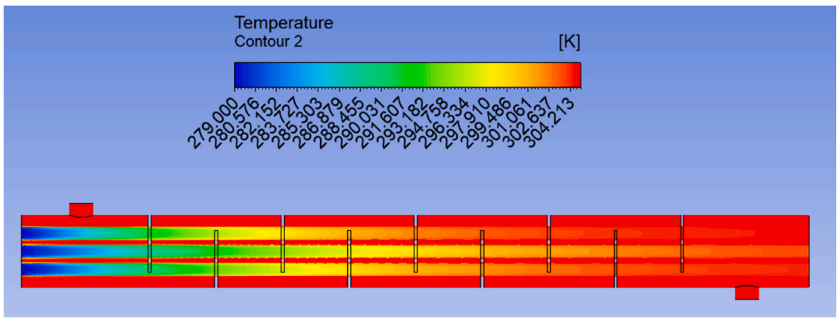

Fig. 12. Temperature distribution of the system interval = 110 mm, Flowrate = 1.3 kg/h.

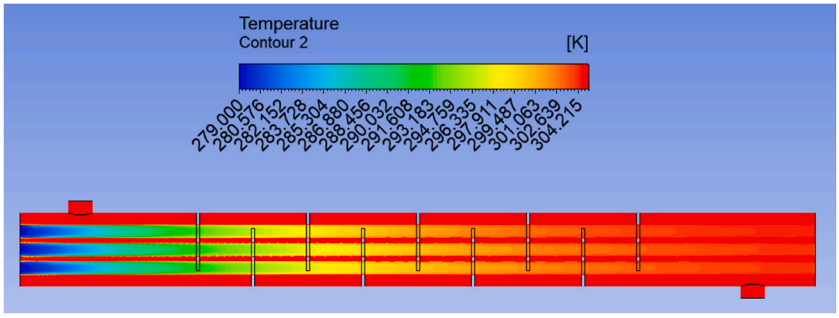

Fig. 13. Temperature distribution of the system interval = 90 mm, Flowrate = 1.7 kg/h.

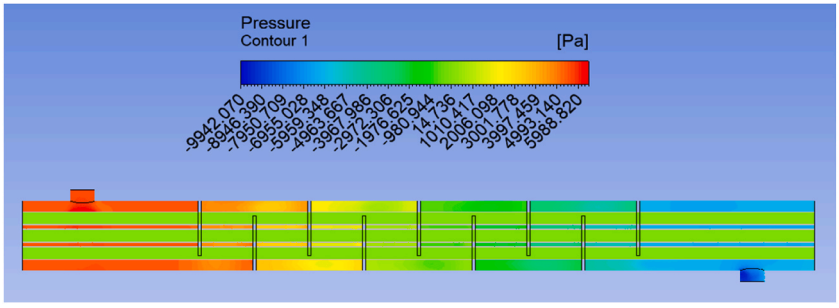

Fig. 14. Pressure distribution of the system interval = 90 mm, Flowrate = 1.7 kg/h.

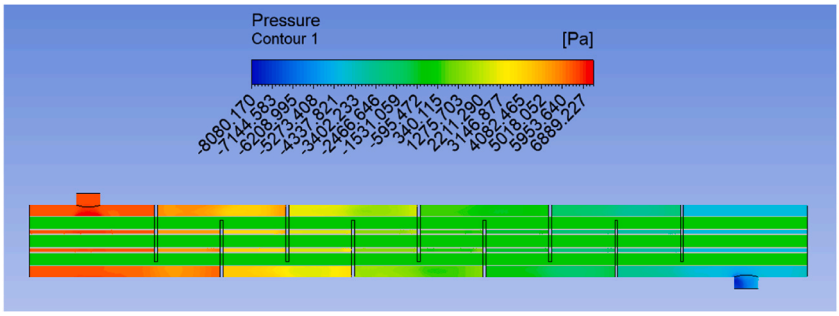

Fig. 15. Pressure distribution of the system interval = 110 mm, Flowrate = 1.7 kg/h.

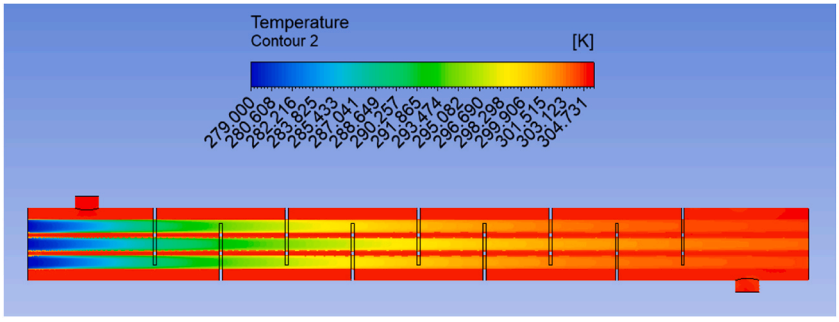

Fig. 16. Temperature distribution of the system interval = 110 mm, Flowrate = 1.7 kg/h.

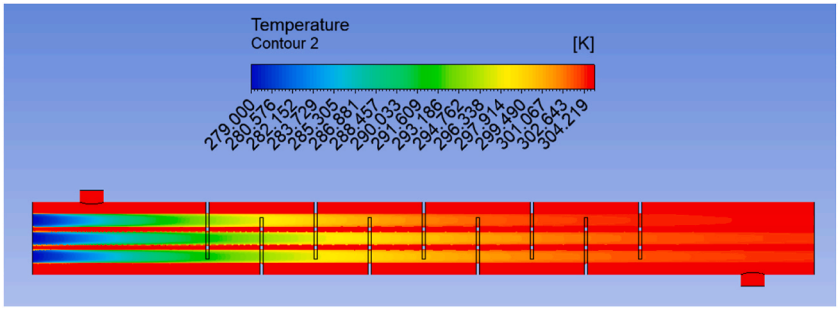

Fig. 17. Temperature distribution of the system interval = 90 mm, Flowrate = 1.9 kg/h.

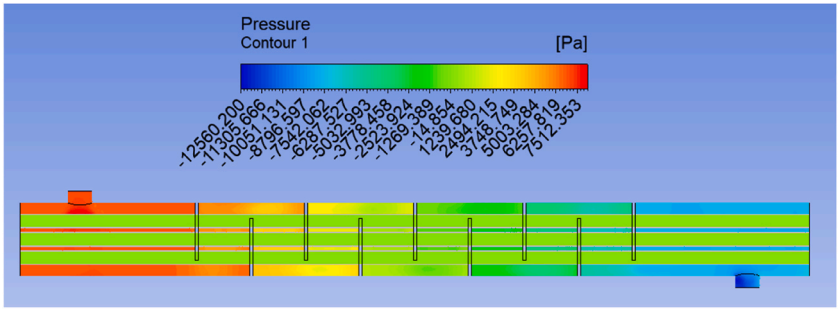

Fig. 18. Pressure distribution of the system interval = 90 mm, Flowrate = 1.9 kg/h.

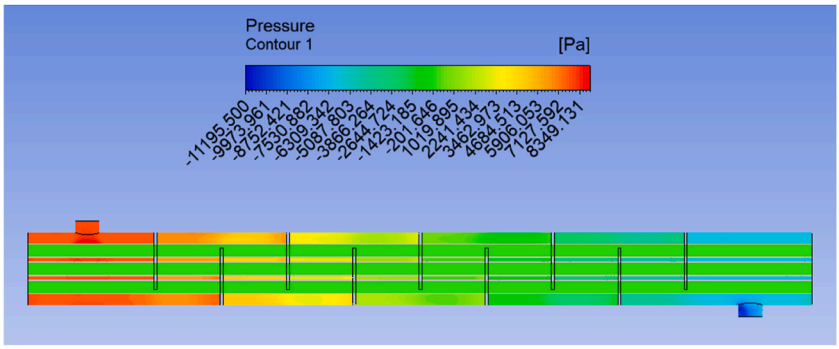

Fig. 19. Pressure distribution of the system interval = 110 mm, Flowrate = 1.9 kg/h.

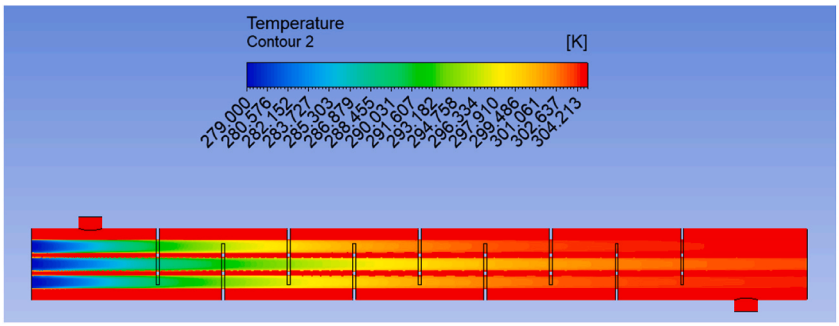

Fig. 20. Temperature distribution of the system interval = 110 mm, Flowrate = 1.9 kg/h.

heat exchange. It is observed that the water warms up to approximately 304,212 °C. In this case, as the flow rate remained constant and the baffle gap changed, the thermal performance values changed positively.

According to Fig. 6, while the pressure on the pipe side at the inlet is observed on the green scale, when the flow rate is 0.9 kg/h and the baffle gap is 90 mm, the cold water interacts with the hot water and due to heat exchange, the cold water heats up towards the outlet and reaches approximately 1774.225 Pa. It is observed that it is in the blue scale region.

In the other case, according to Fig. 7, it is observed that the pressure on the inlet side is in the green zone, while cold water interacts with hot water when the flow rate is 0.9 kg/h and the baffle gap is 110 mm, It is observed that the pressure of the cold water towards the outlet is heated to approximately 1950,220 °C due to the heat exchange.

Simulation consequences of temperature and pressure dissipation were transferred to the study. Therefore, 90 mm intervals and 0.9 kg/h FR is shown in Figs. 5 and 6. In addition, temperature and pressure dissipation at 110 mm intervals at 0.9 kg/h FR is shown in Figs. 7 and 8. When topographic building of temperature dissipation is investigated, differences come in view. It is shown that Fig. 8's temperature dissipation is in a more homogenized state than Fig. 5. Moreover, about the pressure dissipation, it is shown that Fig. 6's pressure dissipation is higher than Fig. 7.

According to Fig. 9, while the pressure on the pipe side at the inlet is observed on a green-red scale, cold water interacts with hot water when the flow rate is 1.3 kg/h and the baffle gap is 90 mm, and it is observed that the cold water towards the outlet heats up due to the heat exchange and reaches approximately 307,013 Pa in the green scale region.

In the other case, according to Fig. 11, it is observed that the pressure on the inlet side is in the orange region, while cold water interacts with hot water when the flow rate is 1.3 kg/h and the baffle gap is 110 mm, and It is observed that the pressure of the cold water towards the outlet heats up and increases to approximately 986 Pa due to the heat exchange. As a result of the analysis, an increase in pressure values was observed as the flow rate increased from 0.9 kg/h to 1.3 kg/h and the baffle gap increased. If the pressure values increase excessively, it may cause increased leaks.

According to Fig. 10, while the water temperature at the inlet side is between 279,100 °C and 285,304 °C, when the flow rate is 1.3 kg/h and the baffle gap is 90 mm, the cold water interacts with the hot water and the cold water towards the outlet heats up to about approx. It is observed that it reaches 304,217 °C.

In the other case, according to Fig. 12, while the water temperature at the inlet side is between 279,000 °C and 288,455 °C, when the flow rate is 1.3 kg/h and the baffle gap is 110 mm, the cold water interacts with the hot water and cold water towards the outlet due to heat exchange. It is observed that the water warms up to approximately 304,213 °C. In this case, as the flow rate remained constant and the baffle gap changed, the thermal performance values changed positively.

Simulation consequences of temperature and pressure dissipation were transferred to the study. Therefore, 90 mm intervals and 1.3 kg/h FR is shown in Figs. 9 and 10. In addition, temperature and pressure dissipation at 110 mm intervals at 1.3 kg/h FR is shown in Figs. 11 and 12. When topographic building of temperature dissipation is investigated, differences come in view. It is shown that Fig. 10's temperature dissipation is in a more homogenized state than Fig. 12. Moreover, about the pressure dissipation, it is shown that Fig. 9's pressure dissipation is higher than Fig. 11.

According to Fig. 13, while the water temperature on the inlet side is between 279,200 °C and 290,032 °C, cold water interacts with hot water when the flow rate is 1.7 kg/h and the baffle gap is 90 mm, and it is observed that the cold water towards the outlet heats up and reaches approximately 304,198 °C due to the heat exchange.

In the other case, according to Fig. 16, while the water temperature on the inlet side is between 279,000 °C and 293,474 °C, the cold water interacts with the hot water when the flow rate is 1.7 kg/h and the baffle gap is 110 mm, and it is observed that the cold water towards the outlet heats up and reaches approximately 304,731 °C due to the heat exchange. In this case, as the flow rate remained constant and the baffle gap changed, the thermal performance values changed positively.

According to Fig. 14, while the pressure on the pipe side at the inlet is observed on average in a green-orange scale, cold water interacts with hot water when the flow rate is 1.7 kg/h and the baffle gap is 90 mm, and it is observed that due to the heat exchange, the cold water towards the outlet heats up and reaches a temperature of approximately 1010.417 Pa in the green scale region.

In the other case, according to Fig. 15, it is observed that the pressure on the inlet side is in the orange region, while the cold water interacts with the hot water when the flow rate is 1.7 kg/h and the baffle gap is 110 mm, and it is observed that the pressure of the cold water towards the outlet heats up and increases to approximately 1275.703 Pa due to the heat exchange. As a result of the analysis, an increase in pressure values was observed as the flow rate increased from 0.9 kg/h to 1.7 kg/h and the baffle gap increased.

Simulation consequences of temperature and pressure dissipation were transferred to the study. Therefore, 90 mm intervals and 1.7 kg/h FR is shown in Figs. 13 and 14. In addition, temperature and pressure dissipation at 110 mm intervals at 1.7 kg/h FR is shown in Figs. 15 and 16. When topographic building of temperature dissipation is investigated, differences come in view. It is shown that Fig. 13's temperature dissipation is in a more homogenized state than Fig. 16. Moreover, about the pressure dissipation, it is shown that Fig. 15's pressure dissipation is higher than Fig. 14.

According to Fig. 17, while the water temperature on the inlet side is between 279,100 °C and 291,050 °C, cold water interacts with hot water when the flow rate is 1.9 kg/h and the baffle gap is 90 mm, and it is observed that the cold water towards the outlet heats up to approximately 304.219 °C due to the heat exchange.

In the other case, according to Fig. 20, while the water temperature on the inlet side is between 279,000 °C and 293,500 °C, the cold water interacts with the hot water when the flow rate is 1.9 kg/h and the baffle gap is 110 mm, and it is observed that the cold water towards the outlet heats up to approximately 304,213 °C due to the heat exchange. In this case, as the flow rate remained constant and the baffle gap changed, the thermal performance values changed positively.

According to Fig. 18, while the pressure on the pipe side at the inlet is observed on average in a green-orange scale, cold water interacts with hot water when the flow rate is 1.9 kg/h and the baffle gap is 90 mm, and it is observed that due to the heat exchange, the

cold water towards the outlet heats up and reaches a temperature of approximately 1239,680 Pa in the green scale region.

In the other case, according to Fig. 19, it is observed that the pressure on the inlet side is in the green-orange region, while the cold water interacts with the hot water when the flow rate is 1.9 kg/h and the baffle gap is 110 mm, and it is observed that the pressure of the cold water towards the outlet heats up and increases to approximately 1850.00 Pa due to the heat exchange. As a result of the analysis, an increase in pressure values was observed as the flow rate increased from 0.9 kg/h to 1.9 kg/h and the baffle gap increased. If the pressure values increase excessively, it may cause increased leaks and may also have an effect on sediment formation.

Simulation consequences of temperature and pressure dissipation were transferred to the study. Therefore, 90 mm intervals and 1.9 kg/h FR is shown in Figs. 17 and 18. In addition, temperature and pressure dissipation at 110 mm intervals at 1.9 kg/h FR is shown in Figs. 19 and 20. When topographic building of temperature dissipation is investigated, differences come in view. It is shown that Fig. 17's temperature dissipation is in a more homogenized state than Fig. 20. Moreover, about the pressure dissipation, it is shown that Fig. 19's pressure dissipation is higher than Fig. 18.

According to Fig. 21, it can be seen that the HCO value can reach different values by changing FR. By including BFF spacing into the analysis as a variable factor, results as shown in Fig. 21 were obtained. In the analysis, the interval values were 90 mm and 110 mm, and the changes in FR values of 0.9 kg/h, 1.3 kg/h, 1.7 kg/h and 1.9 kg/h increased in direct proportion. If FR was 1.3 kg/h and the spacing value was 110 mm, the HCO value was obtained to be lower than the situation that would occur if the spacing value was 90 mm. If the HCO value was 1.9 kg/h and the spacing value was 90 mm, the HCO value was obtained to be higher than the situation that would occur if the spacing value was 110 mm.

According to Fig. 22, it can be seen that PD value can reach different values as FR changes. By including the BFF spacing into the analysis as a variable factor, results as shown in Fig. 22 were obtained. In the analysis, the interval values were 90 mm and 110 mm, and the changes in FR values of 0.9 kg/h, 1.3 kg/h, 1.7 kg/h and 1.9 kg/h increased in direct proportion. If FR was 0.9 kg/h and the gap value was 110 mm, PD value was obtained to be higher than the situation that would occur if the gap value was 90 mm. If FR was 1.7 kg/h and the spacing value was 90 mm, PD value was obtained to be lower than the situation that would occur if the spacing value was 110 mm.

According to Fig. 23, it can be seen that the HPD value can reach different values by changing FR. By including BFF spacing into the analysis as a variable factor, results as shown in Fig. 23 were obtained. In the analysis, the interval values were 90 mm and 110 mm, and the changes in FR values of 0.9 kg/h, 1.3 kg/h, 1.7 kg/h and 1.9 kg/h decreased in direct proportion. If FR was 1.3 kg/h and the gap value was 110 mm, PD value was obtained to be lower than the situation that would occur if the gap value was 90 mm. If FR was 1.7 kg/h and the gap value was 90 mm, PD value was obtained to be higher than the situation that would occur if the gap value was 110 mm.

4. Conclusions

The effects of changing plate spacings on the total heat transfer performance and PD in the aforethought system were examined. The results obtained by taking into account the variable factors along with the mass flow factor of the change in the plate spacings were transferred to the study and followed with figures. In the study, firstly, the results of HCO obtained by changing the MRA and range were monitored. The smallest value of the heat transfer rate was obtained at 110 mm plate spacing and 0.9 kg/h FR. In addition, if the plate spacing was 90 mm, the smallest HCO was obtained at 0.9 kg/h. The highest HCO was obtained when the plate spacing was 90 mm and FR was 1.9 kg/h. Therefore, it would be better to choose a system with a plate spacing of 90 mm and a FR of 1.9 kg/h in terms of efficiency and thermal yielding.

In the second part of the study, the results of PD obtained by changing the MRA and gap were monitored. The results obtained by taking into account the variable factors along with the mass flow factor of the change in the plate spacings were transferred to the study and followed with figures. The smallest value of PD level was obtained at 90 mm plate spacing and 0.9 kg/h FR. In addition, if the plate

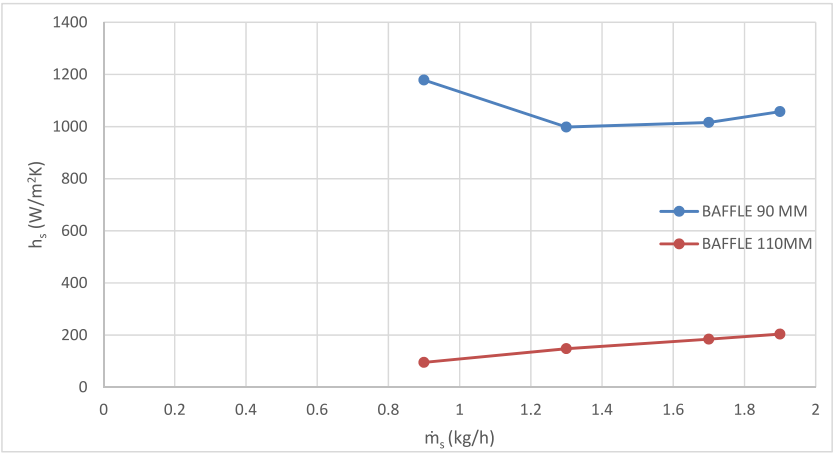

Fig. 21. Variation of HCO with flowrate.

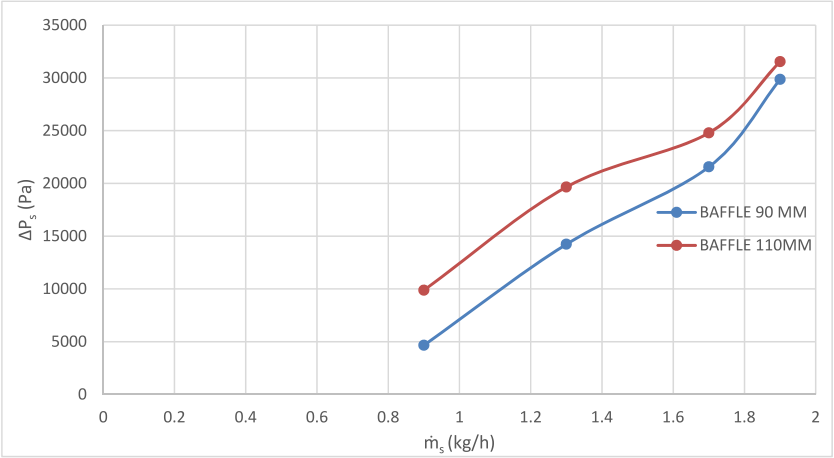

Fig. 22. Variation of Pressure drop with flowrate.

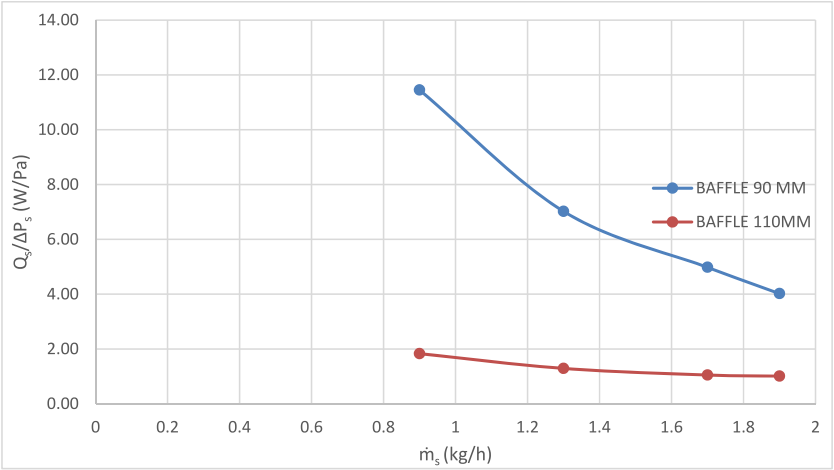

Fig. 23. Variation of HPD with flowrate.

spacing was 110 mm, the smallest HCO was obtained at 0.9 kg/h. The largest PD value was obtained when the plate spacing was 110 mm and FR was 1.9 kg/h. Therefore, choosing a system with a plate spacing of 90 mm and a FR of 0.9 kg/h would be more accurate in terms of efficiency, thermal yielding and pressure balancing.

In the last part of the study, the results obtained by changing the MRA and range of the HPD value were monitored. The results obtained by taking into account the variable factors along with the mass flow factor of the change in the plate spacings were transferred to the study and followed with figures. The smallest value of the HPD level was obtained at 110 mm plate spacing and 1.9 kg/h FR. In addition, if the plate spacing was 90 mm, the smallest HPD value was obtained at 1.9 kg/h. The highest HPD value was obtained when the plate spacing was 90 mm and FR was 0.9 kg/h. Therefore, choosing a system with a plate spacing of 90 mm and a FR of 0.9 kg/h will be more efficient in terms of thermohydraulic performance and pressure balancing. As a result, it was concluded that if the plate spacing was selected as 90 mm, it could be improved by 15 % compared to the system design with 110 mm plate spacing.

Declaration of competing interest

The authors declare that they have no known competing financial interests or personal relationships that could have appeared to influence the work reported in this paper.

Data availability

Data will be made available on request.

Acknowledgements

This research did not receive any specifc grant from funding agencies in the public, commercial, or not-for-profit sector.

Nomenclature

STH(x)	Shell-and-tube heat exchanger(s)
CFD	Computational fluid dynamics
L/D	Tube length in meters/Diameter of shell in meter
EDN	Entransy dissipation number
hs	Convective heat transfer coefficient in kW/m^2K
HX(es)	Heat exchanger(s)
HCO	Heat transfer coefficient $[W/m^2K]$
MRA	Mass flow rate [kg/h]
HPD	Heat transfer rate per pressure drop [W/Pa]
FR	Flow rate
BFF	Baffle plate
PD	Pressure drop
Pr	Prandlt number
k	Turbulent kinetic energy ($m^2 \bullet s^{-2}$)
T	Temperature (K)
C	Capacity ratio
ΔP	Pressure drop (Pa)
N	Number of shell passes
c_p	Specific heat capacity ($J.kg^{-1}.K^{-1}$)
C_1, C_2, n	Coefficients of Wilson plots
A	Heat transfer area (m^2)
V	Flow velocity ($m.s^{-1}$)

Greek Symbols

ρ	Density in m^3/kg
ε	Heat balance deviation or turbulence kinetic energy dissipation rate (m^2s^{-3})

Subscripts

İ	Inlet condition
w	Wall
t	Tube-side
s	shell-side

References

[1] M. Omidi, M. Farhadi, M. Jafari, A comprehensive review on double pipe heat exchangers, Appl. Therm. Eng. 110 (2017) 1075–1090.
[2] Y.H. You, A.W. Fan, S.Y. Huang, W. Liu, Numerical modeling and experimental validation of heat transfer and flow resistance on the shell side of a shell-and-tube heat exchanger with flower baffles, Int. J. Heat Mass Tran. 55 (2012) 7561–7569, https://doi.org/10.1016/j.ijheatmasstransfer.2012.07.058.
[3] Z.F. Huang, A. Nakayama, K. Yang, C. Yang, W. Liu, Enhancing heat transfer in the core flow by using porous medium insert in a tube, Int. J. Heat Mass Tran. 53 (2010) 1164–1174, https://doi.org/10.1016/j.ijheatmasstransfer.2009.10.038.
[4] M.M. Aslam Bhutta, N. Hayat, M.H. Bashir, A.R. Khan, K.N. Ahmad, S. Khan, CFD applications in various heat exchangers design: a review, Appl. Therm. Eng. 32 (2012) 1–12, https://doi.org/10.1016/j.applthermaleng.2011.09.001.
[5] J. Wen, H. Yang, S. Wang, Y. Xue, X. Tong, Experimental investigation on performance comparison for shell-and-tube heat exchangers with different baffles, Int. J. Heat Mass Tran. 84 (2015) 990–997.
[6] J. Chen, X. Lu, Q. Wang, M. Zeng, Experimental investigation on thermal-hydraulic performance of a novel shell-and-tube heat exchanger with unilateral ladder type helical baffles, Appl. Therm. Eng. 161 (2019).
[7] Emad M.S. El-Said, Abdulaziz Mohamed, M.M. Awad, A numerical investigation on heat transfer enhancement and the flow structure in a new type plate heat exchanger using helical flow duct, Cogent Eng 4 (1) (2017), 1396638, https://doi.org/10.1080/23311916.2017.1396638.
[8] J. Wen, H.Z. Yang, S.M. Wang, Y.L. Xue, X. Tong, Experimental investigation on performance comparison for shell-and-tube heat exchangers with different baffles, Int. J. Heat Mass Tran. 84 (2015) 990–997, https://doi.org/10.1016/j.ijheatmasstransfer.2014.12.071.
[9] P. Stehlik, V.V. Wadekar, Different strategies to improve industrial heat exchanger, Heat Tran. Eng. 23 (6) (2002) 36–48.
[10] B.I. Master, K.S. Chunangad, V. Pushpanathan, Fouling mitigation using helixchanger heat exchangers, in: Heat Exchanger Fouling and Cleaning: Fundamentals and Applications, 2003.
[11] Y.P. Chen, W.H. Wang, J.F. Wu, et al., Experimental investigation on performances of trisection helical baffled heat exchangers for oil/water–water heat transfer, Energy Convers. Manag. 101 (2015) 460–469.
[12] M. Saeedan, M. Bahiraei, Effects of geometrical parameters on hydrothermal characteristics of shell-and-tube heat exchanger with helical baffles: numerical investigation, modeling and optimization, Chem. Eng. Res. Des. 96 (2015) 43–53.

[13] M. Bahiraei, M. Hangi, M. Saeedan, et al., A novel application for energy efficiency improvement using nanofluid in shell and tube heat exchanger equipped with helical baffles, Energy 93 (2015) 2229–2240.
[14] A. Geete, A. Bhattacharjee, A. Patwa, et al., Entropy, exergy and entransy analyses on fabricated shell and spiral tube heat exchanger, J. Inst. Eng. India Ser. C 102 (2021) 897–908, https://doi.org/10.1007/s40032-021-00686-8.
[15] Ankur Geete, Vivek Patel, Sudarshan S. Tanwar, Shubham Kushwah, Naveen S. Lodhi, Vikash Kushwah, Thermodynamic analysis of designed and fabricated shell- and tube-type heat exchanger by DSTHE software: Kern method, Int. J. Ambient Energy 39 (4) (2018) 343–351, https://doi.org/10.1080/01430750.2017.1303637.
[16] Deepak Malakar, Ankur Geete, Application of entropy and entransy concepts to design shell and tube type surface condenser at different 4L/D ratios for Maral Overseas Ltd, Int. J. Ambient Energy 41 (7) (2020) 813–822, https://doi.org/10.1080/01430750.2018.1490353.
[17] B. Gao, Q. Bi, Z. Nie, J. Wu, Experimental study of effects of baffle helix angle on shell-side performance of shell-and-tube heat exchangers with discontinuous helical baffles, Exp. Therm. Fluid Sci. 68 (2015) 48–57.
[18] S. Zeyninejad Movassag, F. Nemati Taher, K. Razmi, R. Tasouji Azar, Tube bundle replacement for segmental and helical shell and tube heat exchangers: performance comparison and fouling investigation on the shell side, Appl. Therm. Eng. 51 (1) (2013) 1162–1169.
[19] Y.G. Lei, Y.L. He, P. Chu, R. Li, Design and optimization of heat exchangers with helical baffles, Chem. Eng. Sci. 63 (17) (2008) 4386–4395.
[20] A. Swain, M.K. Das, Convective heat transfer and pressure drop over elliptical and flattened tube, Heat Transfer—Asian Res. 45 (5) (2016) 462–481.
[21] Muharrem Hilmi Aksoy, "Santrifüj Pompa Çarkındaki Akış Karakteristiklerinin HAD Ve PIV Yöntemi İle İncelenmesi", Doktora Tezi, Selçuk Üniversitesi, Türkiye, 2018.